

Detecting Batch Heterogeneity via Likelihood Clustering

Austin Talbot

*Pillar Biosciences Inc
Natick, MA, USA*

TALBOTA@PILLARBIOSCI.COM

Yue Ke

*Pillar Biosciences Inc
Natick, MA, USA*

KEY@PILLARBIOSCI.COM

Abstract

Batch effects represent a major confounder in genomic diagnostics. In copy number variant (CNV) detection from next-generation sequencing, many algorithms compare read depth between test samples and a reference derived from the processing batch, assuming samples are process-matched. When this assumption is violated, with causes ranging from reagent lot changes and sample quality differences to multi-site processing, the reference becomes inappropriate, introducing false CNV calls or masking true pathogenic variants. Detecting such heterogeneity before downstream analysis is critical for reliable clinical interpretation. Existing batch effect detection methods either cluster samples based on raw features, risking conflation of biological signal with technical variation, or require known batch labels that are frequently unavailable. We introduce a method that addresses both limitations by clustering samples according to their Bayesian model evidence. The central insight is that evidence quantifies compatibility between data and model assumptions, technical artifacts violate assumptions and reduce evidence, whereas biological variation, including CNV status, is anticipated by the model and yields high evidence. This asymmetry provides a discriminative signal that separates batch effects from biology. We formalize heterogeneity detection as a likelihood ratio test for mixture structure in evidence space, using parametric bootstrap calibration to ensure conservative false positive rates. We validate our approach on synthetic data demonstrating proper Type I error control, three clinical targeted sequencing panels (liquid biopsy, BRCA, and thalassemia) exhibiting distinct batch effect mechanisms, and mouse electrophysiology recordings demonstrating cross-modality generalization. Our method achieves superior clustering accuracy compared to standard correlation-based and dimensionality-reduction approaches while maintaining the conservativeness required for clinical usage.

1. Introduction

Batch effects are a persistent source of error in genomic diagnostics (Leek et al., 2010; Johnson et al., 2007). In copy number variant (CNV) detection from next-generation sequencing (NGS), many methods compare read depth between a test sample and a reference derived from the processing batch (Fromer et al., 2012; Krumm et al., 2012; Alkan et al., 2011). This approach assumes that samples within a batch are process-matched, that is they are prepared under identical conditions, sequenced with the same reagents on the same instrument run, and analyzed through the same bioinformatics pipeline, so that the reference captures technical variation unrelated to copy number. When this assumption is

violated, the batch reference becomes inappropriate, introducing spurious CNV calls that may trigger unnecessary invasive procedures or, conversely, mask true pathogenic variants that would otherwise prompt clinical intervention (Risso et al., 2014; Kuśmirek et al., 2019). Detecting such heterogeneity before downstream analysis is performed is critical for reliable diagnostics.

Existing approaches to batch effect detection fall broadly into two categories. Unsupervised methods cluster samples based on raw features, such as principal components of read counts or coverage profiles, and flag clusters that correlate with technical covariates (Leek and Storey, 2007). However, these methods are prone to confounding biological signal with technical variation: a cluster of samples carrying true CNVs may be misidentified as a batch artifact, leading to unnecessary re-processing or exclusion of valid data. Supervised methods assess the association between known batch labels and molecular measurements (Johnson et al., 2007), but in clinical sequencing workflows, batch membership is often unknown or incompletely recorded.

A practical heterogeneity detection method must satisfy several competing criteria. First, it must be conservative: in clinical settings, flagging a batch as heterogeneous triggers costly re-sequencing or manual review, so false alarms carry real operational burden. Second, it must be sensitive to diverse technical effects, not just systematic shifts in coverage, but also increased variance, outlier amplicons, or subtle changes in noise structure that manifest differently across samples. Third, and most critically, it must distinguish technical artifacts from true biological signal: a method that flags batches simply because they contain CNV-positive samples would be counterproductive, as CNVs are precisely what we aim to detect. Fourth, it must be robust to individual outliers, a single failed sample should be flagged as such, not interpreted as evidence of global batch structure. Satisfying all four criteria simultaneously is challenging: sensitive methods tend to over-detect structure, conservative methods miss subtle effects, and standard clustering approaches cannot distinguish technical from biological heterogeneity.

We introduce a heterogeneity detection method that addresses these challenges by clustering samples according to their Bayesian model evidence (marginal likelihood), which quantifies how well the assumed statistical model explains each sample’s data (Kass and Raftery, 1995; MacKay, 2003). The key insight is that model evidence measures compatibility between data and model assumptions, not merely goodness of fit to a point estimate. A CNV detection model is designed to explain samples with copy number changes; true CNV-positive samples are well-modeled and yield high evidence. In contrast, technical artifacts, such as reagent degradation, pipetting errors, or reference mismatch, which introduce noise patterns that the model does not anticipate, violate its assumptions and systematically reduce evidence. This asymmetry allows evidence to serve as a discriminative signal as low evidence indicates unexpected behavior (assumption violations), while biological variation produces expected behavior that the model handles well. By examining the distribution of evidence values across a cohort rather than clustering on raw features, we isolate the signal of technical heterogeneity from the signal of biological variation.

In this work, we demonstrate our method on synthetic data as well as three different assays, each detecting a distinct source of batch effects. Furthermore, we demonstrate that our method is broadly applicable, detecting batch effects in mouse electrophysiology. We show that our method reliably detects a wide range of sources of heterogeneity, while

avoiding false positives when such effects are known to not exist. We also show that the model evidence outperforms alternative methods for distinguishing the groups when batch effects are present.

The contents of this work are as follows. In Section 2, we summarize related work for detecting and characterizing batch effects. In Section 3, we describe our method, particularly as applied to the task of CNV detection. Section 4 provides an analysis of our method on synthetic data, demonstrating that our test is conservative. Section 5 describes the cohorts on which our method is evaluated, along with feature and processing descriptions. We then analyze these datasets in Section 6. Finally, in Section 7 we provide brief concluding remarks and directions for future research. Python code implementing all models, loading the data used, and scripts required to reproduce all results is available at <https://github.com/Pillar-Biosciences-Inc/BatchDetect>.

Generalizable Insights about Machine Learning in the Context of Healthcare

- **Evidence as a diagnostic signal.** Bayesian model evidence provides a principled, label-agnostic measure of assumption violation. Unlike prediction error or reconstruction loss, evidence integrates over parameter uncertainty and naturally penalizes model misspecification, enabling heterogeneity detection without batch labels and without misclassifying biologically positive samples as artifacts.
- **Distribution shift detection in evidence space.** Framing data quality monitoring as distribution shift detection over model fit as opposed to input features sidesteps the fundamental challenge of disentangling technical from biological variation, a problem that confounds many alternative approaches.
- **Calibrated hypothesis testing for structure detection.** The parametric bootstrap framework for testing mixture structure is broadly applicable: any clinical ML pipeline that computes per-sample likelihoods can incorporate this approach to monitor for batch effects or data drift, with rigorous false discovery control.

2. Related Work

Batch effects have long been recognized as a major confounder in genomic analyses (Leek et al., 2010). In CNV detection, several methods mitigate batch-specific noise through dynamic reference selection. ExomeDepth (Plagnol et al., 2012) constructs reference panels from samples with maximal read-depth correlation; CLAMMS (Packer et al., 2016) and CANOES (Backenroth et al., 2014) employ similar strategies. These approaches can substantially improve CNV calling accuracy, particularly in targeted panels where sample-to-sample variability is high (Kuśmirek et al., 2019). However, reference-selection methods operate reactively—they optimize the reference for each sample but do not explicitly identify whether batch heterogeneity exists. When unrecognized subgroups are present, correlation-based selection may still construct inappropriate references, propagating systematic errors. Grouping samples by known batch labels (e.g., library preparation date) prior to calling can reduce false positives (Krumm et al., 2012), but this requires metadata that is not always available or reliable.

In contrast to the mature literature on batch correction, formally detecting batch heterogeneity (i.e., deciding whether correction is warranted) has received less attention. Existing approaches include variance-attribution heuristics such as PVCA (Li et al., 2009), supervised PCA-based tests such as gPCA (Reese et al., 2013), related distributional tests (e.g., quantra (Hicks and Irizarry, 2015)) and single-cell mixing scores (e.g., kBET (Büttner et al., 2019)) have also been proposed. However, in the clinical genomics regime, $p \gg n$ with small batches ($n \approx 20\text{--}30$), covariance-driven methods become unstable, distance-based methods suffer from high-dimensional concentration and dispersion confounding, and permutation tests provide coarse p -value resolution.

3. Methods

Our principal focus is targeted amplicon sequencing for CNV detection. In this assay, predefined genomic loci (amplicons) are PCR-amplified and sequenced; the resulting read counts are approximately proportional to underlying copy number, with variability arising from PCR efficiency, sample effects, and sequencing noise.

Let J denote the number of targeted amplicons retained after quality control for a given sample. For amplicon $j \in \{1, \dots, J\}$, we observe a read count s_j from the test sample and a corresponding count n_j from a process-matched reference. In practice, n_j may denote either (i) counts from a matched normal processed under comparable conditions, (ii) a summary (e.g., median) across a set of normal samples processed together, or (iii) a summary across the entire batch (normal-free calling); we use the term reference to encompass both cases. We form log ratios

$$\tilde{y}_j = \log(s_j) - \log(n_j). \quad (1)$$

Note that amplicons with low counts are filtered in QC, making zero-division errors not applicable.

To remove global differences in sequencing depth and other sample-wide offsets, we center \tilde{y} by subtracting a robust location estimate. Specifically, we set

$$y_j = \tilde{y}_j - \text{median}_{j' \in \mathcal{J}} \tilde{y}_{j'} \quad \text{or} \quad y_j = \tilde{y}_j - \text{median}_{j' \in \mathcal{C}} \tilde{y}_{j'}, \quad (2)$$

where \mathcal{J} is the set of all retained amplicons and $\mathcal{C} \subseteq \mathcal{J}$ is a predefined set of control amplicons known to be copy-neutral. After centering, $y_j \approx 0$ indicates copy neutrality, negative values indicate deletions, and positive values indicate amplifications. We refer to $\{y_j\}_{j=1}^J$ as log copy-number ratios (lCNRs).

3.1. CNV Statistical Models and Evidence Computation

Our heterogeneity-detection method requires a scalar evidence score for each sample that summarizes how compatible that sample's lCNR profile is with a CNV generative model. We employ two CNV models suited to different panel designs, enabling evaluation of evidence-based heterogeneity detection under distinct modeling assumptions. The first model treats amplicons within each gene as conditionally independent replicates and targets gene-level CNVs, appropriate for panels with sparse targets spread across the genome. The second model induces spatial dependence among neighboring amplicons via a state-space formulation, appropriate for densely tiled panels covering a contiguous region (in this work,

BRCA1/2 and thalassemia assays). The two models also differ in inference procedures and in how evidence is estimated.

3.1.1. HIERARCHICAL BAYESIAN MODEL FOR GENE-LEVEL CNV DETECTION

In the gene-level model, amplicons targeting the same gene are treated as noisy measurements of an underlying gene-level ICNR. Let $g \in \{1, \dots, G\}$ index genes, and let y_{ig} denote the ICNR for the i th amplicon targeting gene g . The latent gene-level ICNR is μ_g . We place hierarchical priors on gene-level means and gene-specific scales to share information across genes, and we use a SoftLaplace observation model, a smooth heavy-tailed alternative to the Laplace distribution, to improve robustness to outlier amplicons (Ding, 2014).

The generative model is

$$\begin{aligned} \mu_0 &\sim \mathcal{N}(0, 10), \\ \sigma^2 &\sim \text{InvGamma}(\alpha_\sigma, \beta_\sigma), \\ \tau_0^2 &\sim \text{InvGamma}(\alpha_{\tau_0}, \beta_{\tau_0}), \\ \mu_g \mid \mu_0, \sigma^2 &\sim \mathcal{N}(\mu_0, \sigma^2), \\ z_g &\sim \text{InvGamma}(\alpha_\tau, \beta_\tau), \\ y_{ig} \mid \mu_g, z_g &\sim \text{SoftLaplace}(\mu_g, \tau_0 z_g), \end{aligned} \tag{3}$$

where $\tau_0 z_g$ is a gene-specific scale parameter. The hyperparameters $\{\alpha_\sigma, \beta_\sigma, \alpha_{\tau_0}, \beta_{\tau_0}, \alpha_\tau, \beta_\tau\}$ are fixed a priori to values used in previous work.

We infer the model parameters $\theta = \{\mu_0, \sigma^2, \tau_0^2, \{\mu_g\}_{g=1}^G, \{z_g\}_{g=1}^G\}$ using Hamiltonian Monte Carlo (HMC) (Betancourt, 2017). To estimate the log marginal likelihood $\log p(y)$, we use thermodynamic integration (Calderhead and Girolami, 2009). Let $\tau \in [0, 1]$ denote the inverse temperature, and define the power posterior

$$p_\tau(\theta \mid y) \propto p(y \mid \theta)^\tau p(\theta). \tag{4}$$

Thermodynamic integration uses the identity

$$\ell = \log p(y) = \int_0^1 \mathbb{E}_{\theta \sim p_\tau(\theta \mid y)} [\log p(y \mid \theta)] d\tau. \tag{5}$$

We approximate the integral in (5) by evaluating the expectation at a discrete ladder of inverse temperatures $\{\tau_t\}_{t=1}^T$ spanning $[0, 1]$ and applying the trapezoidal rule. We use 100 temperatures with linear spacing.

3.1.2. STATE-SPACE MODEL FOR SPATIALLY CORRELATED CNV DETECTION

When amplicons target a contiguous genomic region, ICNRs exhibit spatial correlation, and we instead use a state-space model (Chopin et al., 2020). Let x_j denote the latent true ICNR at amplicon j . Spatial dependence is induced via a heavy-tailed innovation model that favors local smoothness while permitting rare large transitions corresponding to CNV boundaries:

$$p(x_{j+1} \mid x_j) = (1 - p) \mathcal{N}(x_j, \epsilon) + p \mathcal{N}(x_j, \sigma^2), \tag{6}$$

where $p \ll 1$ is the probability of a large transition, ϵ controls local smoothness, and $\sigma^2 \gg \epsilon$ permits large jumps. The initial state has a weakly informative prior reflecting the assumption of copy neutrality:

$$x_0 \sim \mathcal{N}(0, \tau_0^2). \quad (7)$$

Observations follow a Laplace likelihood for robustness to outliers:

$$y_j \mid x_j \sim \text{Laplace}(x_j, b). \quad (8)$$

The complete model is

$$\begin{aligned} x_0 &\sim \mathcal{N}(0, \tau_0^2), \\ x_{j+1} \mid x_j &\sim (1-p)\mathcal{N}(x_j, \epsilon) + p\mathcal{N}(x_j, \sigma^2), \\ y_j \mid x_j &\sim \text{Laplace}(x_j, b), \end{aligned} \quad (9)$$

with fixed transition and observation parameters $\theta = \{p, \epsilon, \sigma^2, \tau_0^2, b\}$ chosen a priori for each assay using domain knowledge of expected CNV sizes and noise characteristics (Talbot et al., 2025). Full Bayesian inference over θ is computationally prohibitive for our use case, and we therefore treat θ as fixed when computing evidence.

Inference over latent states $\{x_j\}_{j=0}^J$ proceeds via sequential Monte Carlo using an auxiliary particle filter (Pitt and Shephard, 1999). A standard byproduct of particle filtering is an unbiased estimator of the marginal likelihood. Let M denote the number of particles and let $w_j^{(m)}$ denote the (unnormalized) importance weight for particle m at position j . The particle filter yields the estimator

$$\ell = \log \hat{p}(y \mid \theta) = \sum_{j=1}^J \log \left(\frac{1}{M} \sum_{m=1}^M w_j^{(m)} \right). \quad (10)$$

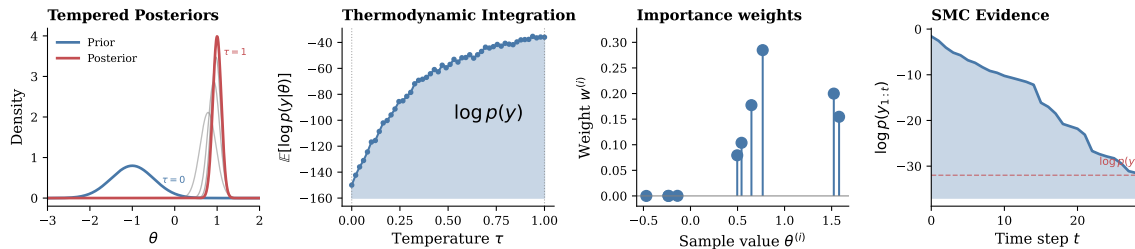


Figure 1: Overview of evidence computation. Left: a sequence of power posteriors indexed by inverse temperature $\tau \in [0, 1]$ used for thermodynamic integration. Second from left: thermodynamic integration estimates $\log p(y)$ by numerically integrating $\mathbb{E}_{p_\tau(\theta|y)}[\log p(y \mid \theta)]$ over τ (Eq. (5)). Middle right: particle-filter weights at a representative amplicon position; highly peaked weight distributions indicate that few particles explain the observation well. Right: particle-filter evidence accumulates across amplicons via the product form in Eq. (10).

3.2. Detecting Batch Heterogeneity via Mixture Modeling of Model Evidence

We compute a normalized evidence score ℓ_i for each sample $i \in \{1, \dots, N\}$ in a cohort. Our core hypothesis is that batch heterogeneity manifests as systematic differences in model compatibility across samples: if a cohort contains two subsets processed under different technical conditions, one subset may be consistently better (or worse) explained by the assumed CNV model, producing a bimodal (or otherwise mixture-like) distribution of $\{\ell_i\}$.

We formalize heterogeneity detection as a likelihood-ratio test comparing a one-component model (homogeneous cohort) to a two-component mixture (heterogeneous cohort). Specifically, we consider

$$\text{Null } (H_0) : \ell_i \sim f(\ell | \mu_1, \alpha_1), \quad (11)$$

$$\text{Alternative } (H_1) : \ell_i \sim \pi f(\ell | \mu_1, \alpha_1) + (1 - \pi) f(\ell | \mu_2, \alpha_2), \quad (12)$$

where $\pi \in (0, 1)$ is the mixture weight and $f(\cdot | \mu, \alpha)$ is a location-scale density. We consider several choices of f which we consider in this work, namely Gaussian, Laplace, hypersecant, t-distribution, and gennorm. We estimate parameters under H_0 and H_1 via expectation-maximization (EM). For the two-component mixture, we initialize EM using k -means centers and perform $n_{\text{init}} = 3$ random restarts, retaining the solution with the highest final log likelihood. Convergence is declared when the change in average log likelihood is below 10^{-4} or after 1000 iterations.

Algorithm 1: Parametric Bootstrap Likelihood Ratio Test in Evidence Space

Input: Evidence scores $\{\ell_i\}_{i=1}^N$, number of bootstrap replicates B

Output: p -value and likelihood ratio statistic LR_{obs}

Fit 1-component generalized normal model $\rightarrow \widehat{M}_0$

Fit 2-component generalized normal mixture $\rightarrow \widehat{M}_1$

$LR_{\text{obs}} \leftarrow 2 \cdot (\mathcal{L}(\{\ell_i\} | \widehat{M}_1) - \mathcal{L}(\{\ell_i\} | \widehat{M}_0))$

for $b \leftarrow 1$ **to** B **do**

 Sample $\{\ell_i^{(b)}\}_{i=1}^N \sim \widehat{M}_0$

 Fit 1-component model to $\{\ell_i^{(b)}\} \rightarrow \widehat{M}_0^{(b)}$

 Fit 2-component mixture to $\{\ell_i^{(b)}\} \rightarrow \widehat{M}_1^{(b)}$

$LR_b \leftarrow 2 \cdot (\mathcal{L}(\{\ell_i^{(b)}\} | \widehat{M}_1^{(b)}) - \mathcal{L}(\{\ell_i^{(b)}\} | \widehat{M}_0^{(b)}))$

end

$$p \leftarrow \frac{1 + \sum_{b=1}^B \mathbb{I}(LR_b \geq LR_{\text{obs}})}{B+1}$$

return p, LR_{obs}

Because finite-mixture models are non-regular (the null hypothesis lies on the boundary of the alternative parameter space), the asymptotic chi-square approximation for the likelihood ratio statistic does not apply (McLachlan and Peel, 2004). We therefore estimate the null distribution of the likelihood ratio statistic via a parametric bootstrap (Davison and Hinkley, 1997).

Let \widehat{M}_0 and \widehat{M}_1 denote the fitted one- and two-component models, respectively, and let $\mathcal{L}(\cdot | M)$ denote the log likelihood under model M . We compute the observed likelihood

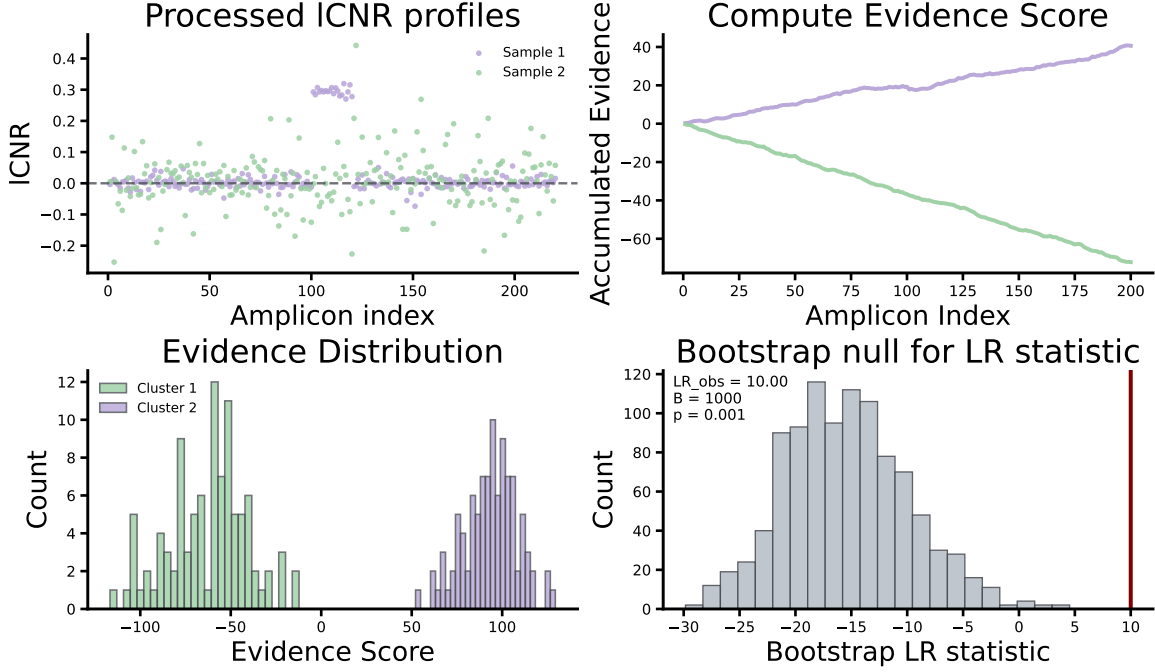


Figure 2: Overview of the proposed heterogeneity detection workflow. On the top left we show two sample LCNRs after preprocessing according to (2). The top right shows an example computation of the evidence, matching the right of Figure 1. Bottom left shows the distribution of the evidences of the samples in the entire batch with a clear bimodal structure and color corresponding to group label. Finally, bottom right visualizes the significance test defined by Algorithm 1.

ratio statistic

$$LR_{obs} = 2 \left(\mathcal{L}(\{\ell_i\} | \widehat{M}_1) - \mathcal{L}(\{\ell_i\} | \widehat{M}_0) \right). \quad (13)$$

For bootstrap replicate $b = 1, \dots, B$ (we use $B = 1000$), we draw an i.i.d. sample

$$\{\ell_i^{(b)}\}_{i=1}^N \sim \widehat{M}_0, \quad (14)$$

refit both one- and two-component models to $\{\ell_i^{(b)}\}$, and compute

$$LR_b = 2 \left(\mathcal{L}(\{\ell_i^{(b)}\} | \widehat{M}_1^{(b)}) - \mathcal{L}(\{\ell_i^{(b)}\} | \widehat{M}_0^{(b)}) \right). \quad (15)$$

We then estimate a finite-sample p -value as

$$p = \frac{1 + \sum_{b=1}^B \mathbb{1}_{LR_b \geq LR_{obs}}}{B + 1}, \quad (16)$$

which includes the observed statistic itself (Davison and Hinkley, 1997). Small p -values indicate that the evidence-score distribution is unlikely to arise from a single homogeneous population, suggesting batch heterogeneity.

4. Synthetic Results: A Conservative Null Distribution

We first assess calibration on synthetic data under a null in which technical batch effects are absent, but biological signal may be present. Specifically, we generate ICNR data from the hierarchical mechanism in (3) using settings matched to a targeted liquid-biopsy panel containing 439 amplicons, including a subset targeting 10 clinically relevant genes. We simulate 1000 independent batches, each comprising $N = 20$ samples. For each simulated batch, we construct a synthetic reference by taking the per-amplicon mean across the batch (the “batch mean” reference), fit the hierarchical CNV model, compute per-sample evidence scores, and apply our heterogeneity detection procedure to obtain a batch-level p -value. We repeat this analysis while varying the component density used in the evidence-space mixture model, comparing five candidates: Gaussian, Student- t with $\nu = 3$, generalized normal (gennorm), Laplace, and hypersecant (sech). This experiment isolates the sensitivity of the downstream mixture test to the choice of evidence-space distribution, holding the data-generating mechanism and evidence computation fixed. We perform a second experiment where we artificially subtract two standard deviations of the “worst” sample, artificially introducing an outlier into the data.

Accurately diagnosing p -value calibration can require many more null replicates than are practical here (Storey and Tibshirani, 2003), because each replicate entails evidence computation for 20 samples and thus thermodynamic integration for 20,000 synthetic cases overall even for the 1000 batches considered here. We therefore adopt two pragmatic criteria that directly target conservativeness at clinically relevant thresholds. First, under a well-calibrated null, p -values are uniformly distributed, i.e., $\text{Beta}(1, 1)$. To summarize departures from uniformity in a parsimonious and interpretable way, we model the empirical p -value distribution as

$$p_i \sim \text{Beta}(a, 1), \quad i = 1, \dots, n, \quad (17)$$

where $a > 1$ indicates conservativeness (density is increasing in p , so small p -values are depleted), $a \approx 1$ indicates approximate calibration, and $a < 1$ indicates anti-conservativeness (small p -values are enriched). With a Gamma prior $a \sim \text{Gamma}(\alpha, \lambda_0)$ (shape α , rate λ_0), the posterior is conjugate. We use the 95% credible interval to quantify uncertainty in a . Second, we place an upper bound on the probability of rejection under the null at 0.05. Let $X = \sum_{i=1}^n \mathbb{1}_{p_i < 0.05}$ denote the number of null batches that would be flagged at a nominal 0.05 threshold. Treating $X \sim \text{Binomial}(n, q)$ with $q = \mathbb{P}(p < 0.05)$ under the null, we compute a Clopper–Pearson upper confidence bound for q (Lehmann and Romano, 2005). This provides a direct, clinically interpretable bound on the false-alarm probability at the operating point used in practice.

Table 1 summarizes both criteria across evidence-space component distributions. We can see that except for the Laplace distribution, all distributions have comparable properties of a nearly uniform distribution under the null, with alpha estimates ranging from 0.9 to 1.01 and the Clopper–Pearson upper interval ranging from 0.025 to 0.07. When we introduced an outlier, however, the situation changed dramatically. Naturally, the Gaussian distribution became highly anti-conservative with $\alpha = 0.25(0.23, 0.27)$, with gennorm and student-t affected to a lesser extent. Surprisingly, the Laplace distribution was the best calibrated of the mixture likelihoods. Figure 4 in the Appendix visualizes the resulting distribution.

For completeness, Appendix B compares our parametric-bootstrap test to a non-bootstrapped alternative, the Lo–Mendell–Rubin (LMR) test (Lo et al., 2001) and Bayesian model selection. We can see in Table 6 that here the component distribution makes a substantial difference, with the hypersecant distribution overly conservative, while the Gaussian and Laplace distributions are highly anti-conservative. As such, the bootstrap procedure is important in clinical applications.

Distribution	No Outlier		Outlier Included	
	Alpha estimate	Clopper-Pearson	Alpha estimate	Clopper-Pearson
Gaussian	0.96 (0.90, 1.02)	0.07	0.25 (0.23, 0.27)	0.73
Hypersecant	0.915 (0.86, 0.97)	0.06	1.53 (1.43, 1.62)	0.06
Student-t	1.01 (0.96, 1.08)	0.025	0.62 (0.58, 0.66)	0.32
Laplace	0.7561 (0.71, 0.8)	0.12	0.94(0.89, 1.00)	0.06
Gennorm	0.93 (0.88, 0.99)	0.05	0.44 (0.41, 0.47)	0.41

Table 1: Effect of mixture distribution on conservativeness

5. Cohort

A detailed description of preprocessing and quality control is provided in Appendix A. Here we summarize the datasets used for evaluation, emphasizing sample sizes, batch factors, and biological signals relevant to batch-effect detection. We consider two modalities: targeted amplicon sequencing (three clinical panels, $n = 24\text{--}100$) and mouse electrophysiology (a combination of two studies with $n = 54$). Key dataset characteristics are summarized in Table 2.

5.1. Targeted Amplicon Sequencing Data

We evaluate three targeted panels spanning distinct, practically relevant batch-effect mechanisms; panel design details and preprocessing are provided in Appendix A.

5.1.1. MULTI-CANCER LIQUID BIOPSY PANEL (LBX)

This dataset comprises 32 FFPE samples sequenced with a 173-amplicon panel designed for low-cost cancer screening (targeting five CNV-associated genes). The batch factor is FFPE preservation quality: 10 libraries were prepared from substantially fragmented FFPE DNA, and 22 from higher-quality clinical FFPE material. This cohort evaluates robustness to amplification-related technical heterogeneity induced by mixed sample quality.

5.1.2. BRCA PANEL

The BRCA dataset targets *BRCA1* and *BRCA2* using 283 amplicons (including normalization controls). The batch factor is reagent lot: 24 samples were sequenced across two lots (lot A: $n = 16$; lot B: $n = 8$), introducing systematic shifts in amplification efficiency and baseline coverage profiles. Biological signal is present via CNVs in 12 samples (six

Table 2: Summary of datasets used for batch effect algorithm validation.

Dataset	N	Batch Factor	Bio. Signal	Validation Purpose
Liquid Biopsy	32	FFPE quality	None	Technical artifact robustness
BRCA Panel	24	Reagent lot	CNV+	Batch vs. biology discrimination
Thalassemia Panel	100	Laboratory	CNV+	Multi-site heterogeneity
Electrophysiology	54	Experiment	Behavior	Cross-modality generalization

with gene-level *BRCA2* gains/losses; six with exon-level *BRCA1* aberrations), enabling assessment of whether heterogeneity is correctly attributed to batch effects rather than true copy-number variation.

5.1.3. THALASSEMIA PANEL

The thalassemia dataset uses a 120-amplicon panel (including normalization controls) targeting the alpha- and beta-globin loci. The batch factor is laboratory origin in a two-site setting (Laboratory A: $n = 58$; Laboratory B: $n = 42$), reflecting multi-site heterogeneity from differences in protocols, reagents, instrumentation, and operator effects. Biological heterogeneity is substantial: 55 samples (55%) carry CNVs affecting the alpha-globin locus, and four additional samples are known poorly-modeled outliers reported in [Talbot et al. \(2025\)](#); we retain these outliers to evaluate behavior under non-ideal model fit. Overall, this cohort evaluates batch-effect detection in a realistic clinical genetics scenario combining multi-site technical variation with strong biological signal.

5.2. Mouse Electrophysiology Data

To assess cross-modality generalization beyond genomics, we include local field potential (LFP) recordings from 54 mice aggregated from two experiments that serve as the batch factor. The first study (SP) recorded LFPs from 26 mice across 8 brain regions during social (paired interaction) and non-social (isolated exploration) conditions ([Mague et al., 2022](#)). The second study (TST) recorded from 28 mice across 11 brain regions during stress-exposure and control conditions; 7 brain regions overlapped with SP ([Talbot et al., 2023](#)). Feature processing is described in Appendix A. Within each experiment, protocols were highly controlled (minimizing intra-experiment batch effects), however, the data in SP was collected in two sequential cohorts. As such, we expect no batch effects in the TST experiment, possible effects in the SP experiment, and likely effects when the data from the two experiments are considered jointly. This dataset therefore evaluates algorithm performance in a setting where batch effects are not reliably diagnosable by visual inspection and where domain shift is expected across experiments.

6. Results

6.1. CNV Heterogeneity Detection

6.1.1. OVERALL PERFORMANCE

In our first analysis, we demonstrate the performance of our method in detecting batch effects in each of the three datasets. We used each of the kernels to evaluate sensitivity to the choice of mixture model, and used 10000 bootstrap iterations for computing the p-values. We also evaluated these p-values on each of the within-batch groups to evaluate the predictions when no batch effects are expected. The results are shown in Table 3.

For the thalassemia and LBX groups, batch effects were significant with every mixture model except hypersecant (thalassemia $p = 0.16$). This conservativeness is to be expected based on our results in Section 4. The p-values were particularly small in thalassemia, which is to be expected due to its relatively large sample size. With the BRCA panel, the results were noticeably weaker, with only the Laplace mixture yielding a significant result. Presumably, the large CNVs combined reduced the ability to distinguish the two groups.

Distribution	BRCA		Thalassemia		LBX FFPE	
	Overall	Subgroups	Overall	Subgroups	Overall	Subgroups
Gaussian	0.070	0.130, 0.477	0.001	0.023, 0.032	0.013	0.352, 0.499
Hypersecant	0.800	0.177, 0.524	0.161	0.069, 0.155	0.007	0.682, 0.108
Student-t	0.077	0.122, 0.477	0.005	0.059, 0.180	0.031	0.303, 0.294
Laplace	0.028	0.057, 0.110	0.001	0.118, 0.650	0.011	0.233, 0.141
Gennorm	0.055	0.092, 0.743	0.001	0.039, 0.101	0.016	0.261, 0.264

Table 3: P-values of the three CNV panels, both the aggregate data with batch effects (Overall), and the two subgroups presumably lacking batch effects (Subgroups).

Notably, however, none of the subgroups with each of these experiments yielded a significant p-value with the lowest p-value for BRCA and the LBX panels being 0.057 and 0.108 respectively. One subgroup in the thalassemia group was borderline significant ($p = 0.04$ for gennorm), but nowhere near the significance level seen in the combined group. This also matches our conclusions on our tests being conservative, even though each group in the thalassemia and BRCA panels have a mixture of positive and negative samples, none are flagged as having batch effects.

6.1.2. STATISTICAL POWER AND SIZE

We then evaluate the statistical power and size of our approach in detecting batch effects on each of these panels as a function of sample sizes. We evaluate the former by repeatedly resampling the data from both groups from sample sizes ranging from 5 to 30, covering the batch sizes we commonly encounter from our customers. To evaluate size, we fit a model with samples coming exclusively from a single group at sample sizes of 12 and 20. The results are shown in Figure 3.

We can see that statistical power is low in all experiments at sample sizes less than 15. However, by 25 and 30 samples power was greater than 0.8. Given that most introductory

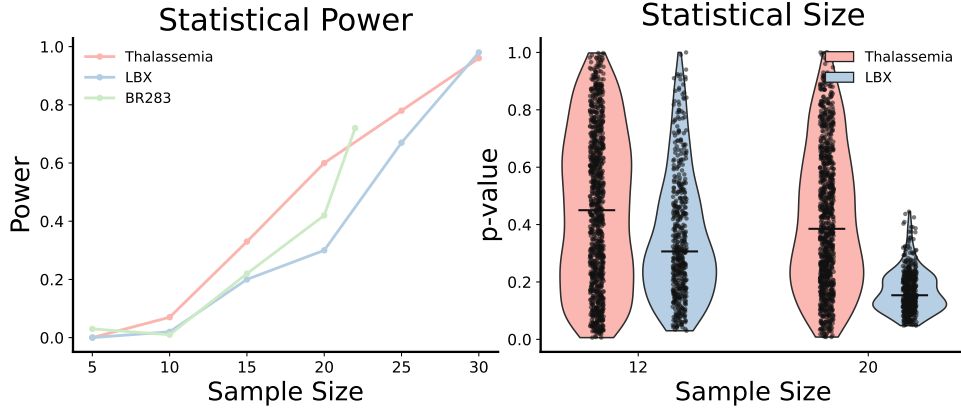


Figure 3: The left figure shows statistical power as a function of sample size in each of the three CNV assays. The right figure shows the distributions of p-values at given sample sizes for the thalassemia and LBX assays.

tests have comparable sample sizes, this is sufficient to determine if the process is sufficiently matched for calling. We also found statistical size was acceptable for thalassemia and LBX at both sample sizes, with a maximum of 4.4% of values being less than 0.05. A plot of the distribution of these p-values is given on the right of Figure 3. The LBX distribution is artificially compressed, likely due to resampling artifacts (selecting a sample size of 20 from 24 samples introduces substantial redundancy).

6.1.3. CLUSTERING ACCURACY

We then evaluate the ability of our method to select comparable samples, allowing us to directly compare to commonly-used methods in the field. We compare our approach against two families of unsupervised advocated for in Kuśmirek et al. (2019). The first family of methods operates directly on self-normalized read count matrices. Given a data matrix $\mathbf{X} \in \mathbb{R}^{n \times p}$ with n samples and p features (e.g., amplicons), we normalize each sample by dividing by its mean count (with a pseudocount of 1 to avoid division by zero). Clustering is then performed either via Gaussian mixture models (GMM), which assume samples arise from a mixture of multivariate Gaussian distributions, or via dimensionality reduction followed by hierarchical clustering. For the latter, we apply principal component analysis (PCA) to the normalized counts, retain the top k components, and cluster the resulting embeddings using Ward’s minimum-variance linkage. We refer to these methods as **GMM** and **PCA-Ward**, respectively.

The second family of methods first computes pairwise sample correlations from the self-normalized counts, yielding a symmetric $n \times n$ correlation matrix \mathbf{R} . We evaluate both Pearson and Spearman correlations, with diagonal elements set to zero to exclude self-similarity. Clusters are then identified using one of three approaches: (1) **Hierarchical**, which converts correlations to distances ($d_{ij} = 1 - r_{ij}$) and applies agglomerative clustering with average linkage; (2) **Spectral**, which constructs an affinity matrix \mathbf{S} with $S_{ij} = \exp(\gamma \cdot$

$\max(r_{ij}, 0)$) and applies spectral embedding followed by k -means; and (3) **PCA-KMeans**, which performs eigendecomposition of the correlation matrix, retains the top eigenvectors as a low-dimensional sample embedding, and applies k -means clustering. All methods require specifying the number of clusters k a priori, which we set to the known value of 2.

Model	BRCA		Thalassemia		LBX FFPE	
	Accuracy	Kappa	Accuracy	Kappa	Accuracy	Kappa
GMM	0.63	0.0	0.78	0.55	0.91	0.76
PCA + Ward	0.63	0.0	0.76	0.51	0.91	0.76
Hierarchical	0.63	0.0	0.78	0.55	0.72	0.13
Spectral	0.71	0.27	0.84	0.66	0.94	0.85
PCA-KMeans	0.63	0.0	0.85	0.68	0.94	0.86
Likelihood (Ours)	0.63	0.34	0.90	0.80	1.0	1.0

Table 4: Batch selection performance of our method to competitors in the BRCA, Thalassemia, and LBX assays.

Our likelihood-based approach achieves the best or tied-best performance across all three targeted sequencing datasets (Table 4). On the LBX FFPE dataset, our method achieves perfect batch classification (accuracy = 1.0, $\kappa = 1.0$), compared to the next-best methods (Spectral and PCA-KMeans) which achieve 0.94 accuracy and $\kappa \leq 0.86$. On the Thalassemia dataset, our method attains 0.90 accuracy and $\kappa = 0.80$, representing a 5–14 percentage point improvement in accuracy and a 12–29 point improvement in Cohen’s κ over all baselines. These gains are particularly notable given that the Thalassemia dataset contains 55% CNV-positive samples, demonstrating that our approach can reliably distinguish laboratory-driven batch effects from biological heterogeneity even when the latter is substantial.

The BRCA dataset presents a uniquely challenging scenario: 12 of 24 samples harbor germline gene-level CNVs in *BRCA2*, which comprises the majority of amplicons in the panel. This biological signal induces strong within-phenotype similarity that cuts across reagent lots, causing most methods to predict the majority class and achieve $\kappa = 0$. While Spectral clustering attains the highest raw accuracy (0.71), it does so with only moderate agreement ($\kappa = 0.27$). In contrast, our likelihood-based method achieves the highest κ (0.34) despite matching the baseline accuracy, indicating that it captures meaningful batch structure rather than simply exploiting class imbalance. This result underscores a key advantage of our approach: by explicitly modeling the generative process underlying read counts, it can disentangle technical batch effects from confounding biological signal where correlation- and distance-based methods fail.

6.2. Mouse LFP Data

Finally, we evaluate our method on two electrophysiology datasets of psychiatric disorders in mice. We use probabilistic principal component analysis (PPCA) as our generative model

of choice, defined as

$$\begin{aligned} p(z) &= N(0, I_L) \\ p(x|z, W, \sigma^2) &= N(Wz, \sigma^2 I) \end{aligned} \quad (18)$$

Unfortunately, the temporal correlation between the observations violate the assumptions of almost all dimensionality-selection techniques, so 20 components were chosen to roughly match the dimensionality used in the original works. This model was fit on a training set of 10 mice from the TST dataset and 5 from the SP dataset. We then evaluated the log likelihood of each observation in the holdout datasets. We then averaged the likelihoods within each mouse within condition, resulting in two observations per mouse. This step was done due to the incredible noise in the observations (the spectral features are incredibly noisy), particularly at low frequencies.

Table 5 summarizes the results. Unsurprisingly, there was incredibly strong evidence of batch heterogeneity when including mice from both experiments, with an average p-value of 0.005. What is interesting is that the TST dataset did not detect batch effects, while SP did. Tail suspension is incredibly stressful and trivial to detect, but our algorithm was not triggered even when the positive and negative conditions were separated. On the other hand, the SP experiment indicated the presence of batch effects ($p = .014$). These mice were recorded in two batches, an initial cohort was augmented by a second cohort several years later. This distinction is maintained, when conditions are separated, but weaker. A potential explanation for this behavior is that the two conditions are nearly indistinguishable, so separating the two conditions increases the variance/sample size without introducing an additional cluster.

Experiment	Conditions Averaged			Conditions Separated		
	Significance	Prob	Avg P-Value	Significance	Prob	Avg P-Value
Social Preference		1.0	0.026		1.0	0.010
Tail Suspension		0.0	0.67		0.0	0.12
Both		1.0	0.011		1.0	0.004

Table 5: Batch effect detection in the electrophysiology data

7. Discussion

Batch effects are a serious concern in many clinical and scientific applications. These issues are particularly acute in CNV detection algorithms requiring normal samples to adjust for amplicon-specific effects. As such, a reliable method for detecting such effects, and potentially selecting process-matched samples is critical. In this work, we develop a novel method for performing this task based on the Bayesian model evidence. This quantity measures how informative a sample is, or equivalently how well the model describes the data, and as such provides a natural metric for detecting a lack of process matching. We show that our method has many desirable properties; it is robust, statistically conservative, and broadly applicable.

References

Can Alkan, Bradley P Coe, and Evan E Eichler. Genome structural variation discovery and genotyping. *Nature reviews genetics*, 12(5):363–376, 2011.

Daniel Backenroth, Jason Homsy, Laura R Murillo, Joe Glessner, Edwin Lin, Martina Brueckner, Richard Lifton, Elizabeth Goldmuntz, Wendy K Chung, and Yufeng Shen. Canoes: detecting rare copy number variants from whole exome sequencing data. *Nucleic acids research*, 42(12):e97–e97, 2014.

Michael Betancourt. A conceptual introduction to hamiltonian monte carlo. *arXiv preprint arXiv:1701.02434*, 2017.

Maren Büttner, Zhichao Miao, F Alexander Wolf, Sarah A Teichmann, and Fabian J Theis. A test metric for assessing single-cell rna-seq batch correction. *Nature methods*, 16(1):43–49, 2019.

Ben Calderhead and Mark Girolami. Estimating bayes factors via thermodynamic integration and population mcmc. *Computational Statistics & Data Analysis*, 53(12):4028–4045, 2009.

Nicolas Chopin, Omiros Papaspiliopoulos, et al. *An introduction to sequential Monte Carlo*. Springer, 2020.

Leon Cohen. *Time-Frequency Analysis*. Prentice Hall Signal Processing Series. Prentice Hall, Englewood Cliffs, NJ, 1995. ISBN 978-0135945322.

Anthony Christopher Davison and David Victor Hinkley. *Bootstrap methods and their application*. Number 1. Cambridge university press, 1997.

Peng Ding. Three occurrences of the hyperbolic-secant distribution. *The American Statistician*, 68(1):32–35, 2014.

Menachem Fromer, Jennifer L Moran, Kimberly Chambert, Eric Banks, Sarah E Bergen, Douglas M Ruderfer, Robert E Handsaker, Steven A McCarroll, Michael C O’Donovan, Michael J Owen, et al. Discovery and statistical genotyping of copy-number variation from whole-exome sequencing depth. *The American Journal of Human Genetics*, 91(4):597–607, 2012. doi: 10.1016/j.ajhg.2012.08.005.

Stephanie C Hicks and Rafael A Irizarry. Quantro: a data-driven approach to guide the choice of an appropriate normalization method. *Genome biology*, 16(1):117, 2015.

W Evan Johnson, Cheng Li, and Ariel Rabinovic. Adjusting batch effects in microarray expression data using empirical bayes methods. *Biostatistics*, 8(1):118–127, 2007.

Robert E Kass and Adrian E Raftery. Bayes factors. *Journal of the american statistical association*, 90(430):773–795, 1995.

Robert E Kass, Uri T Eden, Emery N Brown, et al. *Analysis of neural data*, volume 491. Springer, 2014.

Niklas Krumm, Peter H Sudmant, Arthur Ko, Brian J O’Roak, Maika Malig, Bradley P Coe, Aaron R Quinlan, Deborah A Nickerson, Evan E Eichler, NHLBI Exome Sequencing Project, et al. Copy number variation detection and genotyping from exome sequence data. *Genome research*, 22(8):1525–1532, 2012.

Wiktor Kuśmirek, Agnieszka Szmurło, Marek Wiewiórka, Robert Nowak, and Tomasz Gąbin. Comparison of knn and k-means optimization methods of reference set selection for improved cnv callers performance. *BMC bioinformatics*, 20(1):266, 2019.

Jeffrey T Leek and John D Storey. Capturing heterogeneity in gene expression studies by surrogate variable analysis. *PLoS genetics*, 3(9):e161, 2007.

Jeffrey T Leek, Robert B Scharpf, Héctor Corrada Bravo, David Simcha, Benjamin Langmead, W Evan Johnson, Donald Geman, Keith Baggerly, and Rafael A Irizarry. Tackling the widespread and critical impact of batch effects in high-throughput data. *Nature Reviews Genetics*, 11(10):733–739, 2010.

Erich Leo Lehmann and Joseph P Romano. *Testing statistical hypotheses*. Springer, 2005.

Heng Li. Aligning sequence reads, clone sequences and assembly contigs with bwa-mem. *arXiv preprint arXiv:1303.3997*, 2013.

Jianying Li, Pierre R Bushel, Tzu-Ming Chu, and Russell D Wolfinger. Principal variance components analysis: estimating batch effects in microarray gene expression data. *Batch effects and noise in microarray experiments: sources and solutions*, pages 141–154, 2009.

Yungtai Lo, Nancy R Mendell, and Donald B Rubin. Testing the number of components in a normal mixture. *Biometrika*, 88(3):767–778, 2001.

David JC MacKay. *Information theory, inference and learning algorithms*. Cambridge university press, 2003.

Stephen D Mague, Austin Talbot, Cameron Blount, Kathryn K Walder-Christensen, Lara J Duffney, Elise Adamson, Alexandra L Bey, Nkemdilim Ndubuizu, Gwenaëlle E Thomas, Dalton N Hughes, et al. Brain-wide electrical dynamics encode individual appetitive social behavior. *Neuron*, 110(10):1728–1741, 2022.

Geoffrey McLachlan and David Peel. *Finite Mixture Models*. John Wiley & Sons, 2004.

Jonathan S Packer, Evan K Maxwell, Colm O’Dushlaine, Alexander E Lopez, Frederick E Dewey, Rostislav Chernomorsky, Aris Baras, John D Overton, Lukas Habegger, and Jeffrey G Reid. Clamms: a scalable algorithm for calling common and rare copy number variants from exome sequencing data. *Bioinformatics*, 32(1):133–135, 2016.

Michael K Pitt and Neil Shephard. Filtering via simulation: Auxiliary particle filters. *Journal of the American Statistical Association*, 94(446):590–599, 1999.

Vincent Plagnol, James Curtis, Michael Epstein, Kin Y Mok, Emma Stebbings, Sofia Grigoriadou, Nicholas W Wood, Sophie Hambleton, Siobhan O Burns, Adrian J Thrasher, et al. A robust model for read count data in exome sequencing experiments and implications for copy number variant calling. *Bioinformatics*, 28(21):2747–2754, 2012.

Raquel Prado and Mike West. *Time series: modeling, computation, and inference*. Chapman and Hall/CRC, 2010.

Sarah E Reese, Kellie J Archer, Terry M Therneau, Elizabeth J Atkinson, Celine M Vachon, Mariza De Andrade, Jean-Pierre A Kocher, and Jeanette E Eckel-Passow. A new statistic for identifying batch effects in high-throughput genomic data that uses guided principal component analysis. *Bioinformatics*, 29(22):2877–2883, 2013.

Davide Risso, John Ngai, Terence P Speed, and Sandrine Dudoit. Normalization of rna-seq data using factor analysis of control genes or samples. *Nature biotechnology*, 32(9):896–902, 2014.

Temple F Smith, Michael S Waterman, et al. Identification of common molecular subsequences. *Journal of molecular biology*, 147(1):195–197, 1981.

John D Storey and Robert Tibshirani. Statistical significance for genomewide studies. *Proceedings of the National Academy of Sciences*, 100(16):9440–9445, 2003.

Austin Talbot, David Dunson, Kafui Dzirasa, and David Carlson. Estimating a brain network predictive of stress and genotype with supervised autoencoders. *Journal of the Royal Statistical Society Series C: Applied Statistics*, 72(4):912–936, 2023.

Austin Talbot, Alex Kotlar, Lavanya Rishishiwar, and Yue Ke. Classifying copy number variations using state space modeling of targeted sequencing data: A case study in thalassemia. *arXiv preprint arXiv:2504.10338*, 2025.

Jordy van Enkhuizen, Arpi Minassian, and Jared W. Young. Further evidence for Clock $\Delta 19$ mice as a model for bipolar disorder mania using cross-species tests of exploration and sensorimotor gating. *Behavioural Brain Research*, 249:44–54, jul 2013. ISSN 01664328. doi: 10.1016/j.bbr.2013.04.023.

Peter D Welch. The use of fast fourier transform for the estimation of power spectra: A method based on time averaging over short, modified periodograms. *IEEE Transactions on audio and electroacoustics*, 15(2):70–73, 1967.

Appendix A. Data Processing

Targeted Amplicon Sequencing

We first performed read-to-genome alignment to the GRCh37/hg19 genome using BWA-MEM (Li, 2013). The initial alignment is improved by performing local realignment using Smith-Waterman (Smith et al., 1981) and a proprietary algorithm. To maximize the base accuracy and minimize the sequencing noise, paired-end reads are assembled into consensus reads, weighted with the base quality scores from both mates. The assembled reads correspond to the gene-specific positions on the genome. A set of filters are applied to remove non-uniquely mapped reads (e.g., pseudogenes) and reads that do not match the amplicon positions (e.g., primer-dimers or non-specific amplifications). For CNV calculations, per-amplicon read depth is calculated for each sample. Counts of overlapping amplicons are stored as independent entries.

LIQUID BIOPSY DATA

Our first dataset came from a liquid biopsy panel designed to cover common carcinogenic mutations. It had 173 amplicons targeting a variety of genes, 5 of which were CNV targets.

THALASSEMIA DATA

For the second group, we obtained 44 positive and 13 negative clinical samples as de-identified remnants from a laboratory that tested the samples for clinical use and would have otherwise discarded them. FDA guidance states that such samples may be used for research purposes without obtaining patient consent. These samples were sequenced using a panel of 131 amplicons (of which 11 are excluded gap amplicons) that covers alpha, beta, delta, gamma and epsilon Thalassemia regions, as well as pseudogenes and control regions. Sequencing was performed on an Illumina MiSeqTM platform to an average depth of approximately 2800 paired-end reads. The set of true alpha thalassemia diagnoses were obtained from an orthogonal, clinically validated test that uses MLPA with reflex to GAP-PCR for alpha-thalassemia deletion and duplication detection. Of the positive samples, 31 had a heterozygous alpha-3.7 deletion, 5 had a homozygous alpha-3.7 deletion, 2 had alpha-4.2 deletions, 3 had south-east Asian deletions, 1 sample with an alpha-4.2 duplication, 1 sample with a large HBA duplication, and 1 sample with an alpha-3.7 deletion/4.2 duplication. The second group of samples was obtained similarly from a separate laboratory, and contained 43 samples.

BRCA DATA

To further investigate our quality control metrics, we obtained a second dataset sequenced using a panel designed to detect mutations in the BRCA1 and BRCA2 genes. This panel contains 283 amplicons targeting various regions within BRCA1 and BRCA2 genes, as well as 8 control amplicons from other chromosomes. We obtained four mutation-positive DNA cell line samples from the Coriell Institute for Medical Research with known mutations: NA18949 with a BRCA1 exon 14 and 15 deletion, NA14626 with a BRCA1 exon 12 duplication, NA0330 with a whole-gene duplication of BRCA2, and NA02718 with a whole gene deletion of BRCA2. We also obtained four negative cell line samples NA12878,

NA19240, NA24385, and NA24143. Additionally, Horizon Discovery’s Mimix™ Quantitative Multiplex, fcDNA (Moderate) Reference Standard was used to evaluate performance on Formalin-compromised DNA (FFPE). Libraries were prepared and sequenced on Illumina’s MiSeq™. All samples were collected under informed consent.

Mouse Electrophysiology

TAIL SUSPENSION TEST

The LFPs analyzed in the Tail Suspension Test (TST) came from 26 mice of two genetic backgrounds (14 wild type and 12 Clock- Δ 19). The Clock- Δ 19 genotype has been used to model bipolar disorder (van Enkhuizen et al., 2013). Each mouse was recorded for 20 minutes across 3 behavioral contexts: 5 minutes in its home cage (non-stressful), 5 minutes in an open field (arousing, mildly stressful), and 10 minutes suspended by its tail (highly stressful). Data were recorded from 11 biologically relevant brain regions with 32 electrodes (multiple electrodes per region) at 1000 Hz. These redundant electrodes were implanted to allow for the removal of faulty electrodes and electrodes that missed the target brain region. We chose to average the signals per region to yield an 11-dimensional time series per mouse. This was done because the brain region represents the smallest resolvable location when modeling multiple animals; multiple electrodes function as repeated measurements and averaging allows us to reduce the variance of the measured signal.

We discretized the time series into one-second windows to model how these spectral characteristics change over time. Windows containing saturated signals were removed (typically due to motion artifacts). While there are methods that can characterize the spectral features on a continuous time scale (Prado and West, 2010), the behavior we deal with changes over a longer scale than the observed dynamics. Consequently, it is more effective to discretize and obtain sharper spectral feature estimates (Cohen, 1995) that are more amenable to factor modeling.

We chose to extract the relevant quantities from the recorded data prior to modeling rather than extracting spectral features in the modeling framework for simplicity; the extra modeling step would substantially increase the number of parameters in the model. The features related to power were computed from 1 Hz to 56 Hz in 1 Hz bands using Welch’s method (Welch, 1967), which is recommended in the neuroscience literature (Kass et al., 2014). We chose 56 Hz as a threshold to avoid the substantial noise induced at 60 Hz from the recording equipment, as prior literature has demonstrated that much of the meaningful information is contained in the lower frequencies.

SOCIAL PREFERENCE DATASET

The social preference dataset used identical processing steps as the TST dataset. In this experiment, the mice were placed in a two-chamber assay where the mouse was allowed to wander freely with simultaneous recordings and position tracking for 10 minutes. One chamber included another mouse (social interaction), while the second chamber included an inanimate object (non-social interaction). The original purpose of the study was to characterize the electrophysiology associated with social behavior and causally manipulate these dynamics using optogenetic stimulation. A full description of the methods is given in Mague et al. (2022).

DATA AVAILABILITY

All data from the targeted panels is located on the Github repository associated with this work. The TST dataset can be downloaded at <https://research.repository.duke.edu/concern/datasets/zc77sr31x?locale=en>. For access to the social preference dataset contact the principal investigator, Kafui Dzirasa.

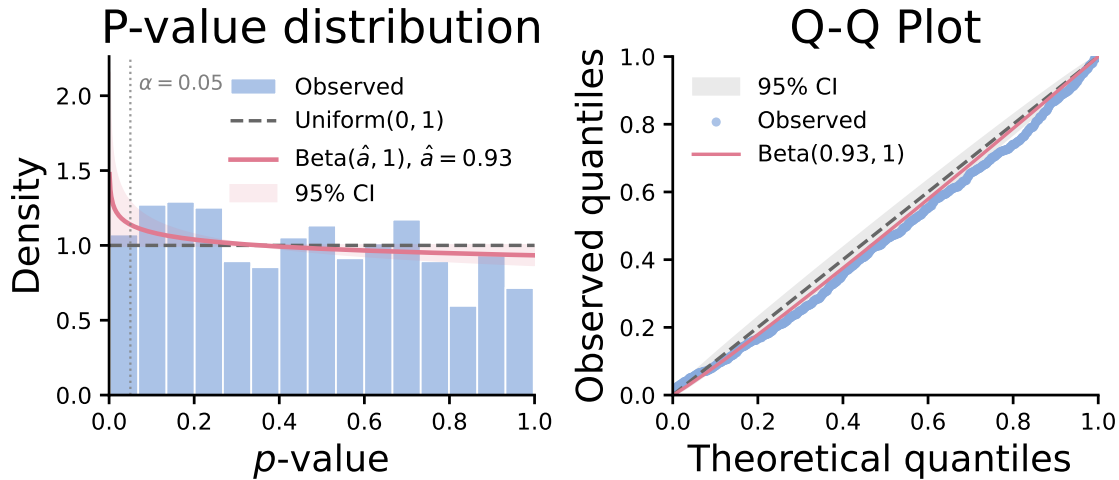


Figure 4: (Left) A histogram of observed p-values (blue) with the theoretical uniform density (dashed gray line) and the fitted $\text{Beta}(\hat{\alpha}, 1)$ distribution overlaid (red) using the gennorm kernel. The shaded region represents the 95% credible interval derived from the posterior uncertainty in $\hat{\alpha}$. (Right) A Q–Q plot comparing observed p-values to expected quantiles from a uniform distribution (dashed gray line) and from the fitted $\text{Beta}(\hat{\alpha}, 1)$ model (red). The gray shaded region denotes the 95% confidence band for order statistics under the null. Systematic deviations from the uniform reference line indicate a departure from the null distribution, consistent with the fitted model.

SYNTHETIC DATA

Distribution	Alpha estimate	Clopper-Pearson
Gaussian	0.49 (0.46, 0.53)	0.23
Hypersecant	21.1 (19.8, 22.0)	0.0056
Student-t	0.71 (0.67, 0.76)	0.11
Laplace	0.37 (0.34, 0.39)	0.39
Gennorm	0.64 (0.60, 0.68)	0.13

Table 6: Effect of mixture distribution on conservativeness

ELECTROPHYSIOLOGY DATA

Experiment	Conditions Averaged			Conditions Separated		
	Significance	Prob	Avg P-Value	Significance	Prob	Avg P-Value
Social Preference	1.0		0.043	1.0		0.043
Tail Suspension	0.75		0.047	0.0		0.56
Both	1.0		0.013	1.0		0.005

Table 7: Batch effect detection in the electrophysiology data using tail suspension data as training set.

Experiment	Conditions Averaged			Conditions Separated		
	Significance	Prob	Avg P-Value	Significance	Prob	Avg P-Value
Social Preference	1.0		0.014	0.63		0.048
Tail Suspension	0.0		0.67	0.0		0.12
Both	1.0		0.013	1.0		0.005

Table 8: Batch effect detection in the electrophysiology data using social data as training set.

Appendix B. Comparison with the LMR Method

We now compare the results of our bootstrap method with the method advocated in [Lo et al. \(2001\)](#).

Distribution	Lo-Mendell-Rubin Adjustment		Bootstrap Calibration	
	Alpha estimate	Clopper-Pearson	Alpha Estimate	Clopper-Pearson
Gaussian	0.49 (0.46, 0.53)	0.22	0.63	0.048
Hypersecant	20.0 (18.7, 21.2)	0.0059	0.0	0.12
Student-t	0.69 (0.65, 0.74)	0.11	1.0	0.005
Laplace	0.37 (0.34, 0.39)	0.39	1.0	0.005
Gennorm	0.63 (0.59, 0.67)	0.14	1.0	0.005

Table 9: A comparison of LMR vs Bootstrap on synthetic data corresponding to liquid biopsy data.